Computers in Biology and Medicine 42 (2012) 1170–1178

Contents lists available at SciVerse ScienceDirect

Computers in Biology and Medicine

journal homepage: www.elsevier.com/locate/cbm

Colorization of CT images to improve tissue contrast for tumor segmentation

Marisol Martinez-Escobar [a], Jung Leng Foo [a,1], Eliot Winer [b,*]

[a] 1620 Howe Hall, Virtual Reality Applications Center, Iowa State University, Ames, IA 50011, United States
[b] Mechanical Engineering and Human-Computer Interaction Department, 1620 Howe Hall, Virtual Reality Applications Center, Iowa State University, Ames, IA 50011, United States

ARTICLE INFO

Article history:
Received 10 October 2011
Accepted 14 September 2012

Keywords:
Colorization
Tumor segmentation

ABSTRACT

Segmenting tumors from grayscale medical image data can be difficult due to the close intensity values between tumor and healthy tissue. This paper presents a study that demonstrates how colorizing CT images prior to segmentation can address this problem. Colorizing the data a priori accentuates the tissue density differences between tumor and healthy tissue, thereby allowing for easier identification of the tumor tissue(s). The method presented allows pixels representing tumor and healthy tissues to be colorized distinctly in an accurate and efficient manner. The associated segmentation process is then tailored to utilize this color data. It is shown that colorization significantly decreases segmentation time and allows the method to be performed on commodity hardware. To show the effectiveness of the method, a basic segmentation method, thresholding, was implemented with and without colorization. To evaluate the method, False Positives (FP) and False Negatives (FN) were calculated from 10 datasets (476 slices) with tumors of varying size and tissue composition. The colorization method demonstrated statistically significant differences for lower FP in nine out of 10 cases and lower FN in five out of 10 datasets.

1. Introduction

When treating tumors in patients, particularly cancerous ones, knowing the size and shape of the tumor is critical. The number of image slices in a CT scan can range from tens to hundreds, thus manually extracting or segmenting these tumors would be a tedious and laborious task due to time and resource constraints. Effective and efficient segmentation routines would have tremendous benefit for a variety of treatment options such as surgery, radiation, and chemotherapy. However, current segmentation methods have a variety of issues precluding them from being used in practical clinical settings including: (1) computational resources, (2) long times to complete segmentation (hours), (3) requiring an atlas of similar cases or training data, and (4) specialization to specific tumor types.

An area of potential to improve tumor segmentation from CT scans would be colorization. The hypothesis proposed is that colorization of the image prior to segmentation will improve the segmentation by increasing the color contrast of neighboring anatomical structures. The goal is to deliver a quick yet effective segmentation solution to be used in a clinical setting. If the accuracy of segmentation methods can be improved further by performing a colorization process, the time and resources required to a full segmentation process can be reduced.

1.1. General image colorization

This section is intended to provide a brief overview of some of the more popular methods being researched before focusing on techniques specific to digital medical data. Many more are being created and refined than can be practically discussed here.

Levin et al. [1] developed a method where a user colorized a selected number of regions of a digital image, and the algorithm propagated the colors through the rest of the image. The colorization process was phrased as an optimization problem by attempting to minimize the color difference between a specific pixel and its neighbors. Welsh et al. [2] developed an automated colorization method in which the color was transferred from a reference color image to a target grayscale image to be colorized. Using statistics, each pixel in the target grayscale image was matched to the color pixels of the color image, usually between 15 s and 4 min. However, colors would bleed into different regions of similar texture. In addition, the need for a reference color image makes the method difficult to use on specialized images such as medical image data. Horiuchi et al. [3] developed

* Corresponding author. Tel.: +1 515 989 1750; fax: +1 515 294 5530.
E-mail addresses: marisol@iastate.edu (M. Martinez-Escobar), foo@iastate.edu (J. Leng Foo), ewiner@iastate.edu (E. Winer).
[1] Tel.: +1 515 294 3092.

0010-4825/$ - see front matter © 2012 Elsevier Ltd. All rights reserved.
http://dx.doi.org/10.1016/j.compbiomed.2012.09.008

a colorization method by placing color seeds in the image and propagating the colors among 4-connected pixels. Qu et al. [4] colorized "manga" (Japanese comics typically printed in black and white) using a level-set method and texture information from the image. The proposed technique was effective on simple regions as well as regions with complex brush strokes, but still required the user to manually "scribble" an initial color in selected regions. Liu et al. [5] developed a probabilistic based segmentation method for colorization. This method worked as a region-based approach to propagate the color, and as a boundary-based approach to detect the edges of the different objects.

Most of the colorization methods reviewed use edge and intensity gradient information to effectively identify regions to apply a defined color. However, medical data imposes constraints that are not addressed in the colorization methods proposed. Medical data such as CT, MRI, and angiograms are often rendered in grayscale, the regions in medical image data are rarely clearly defined, with anatomical structures often blending into each other. The use of a reference images may not be possible, as the anatomy of a patient changes with time, and between different patients. With the complexities of medical images, they will either have to be colorized during acquisition or colorized with more robust techniques.

1.2. Colorized CT images

Most CT images are rendered in grayscale, limiting the amount of information available for segmentation and generally excluding color segmentation methods. Medical images that are rendered in color such as color Doppler, functional MRI, and PET/CT [6] are either too application specific or have not been widely adopted.

Color Doppler imaging [7] produce images of blood flow where different colors and gradients represent the direction of the flow, and velocities respectively. Color Doppler is limited to flow and it is not applicable for rendering images of tumors or organs. A sample screenshot of Color Doppler is shown in Fig. 1a. Functional MRI (fMRI), as shown in Fig. 1b, renders activity in the brain and is used in neurological applications. Neuronal activity causes changes in cerebral blood flow, blood volume, and blood oxygenation. fMRI are rendered by taking the image difference of the activated and rested brain. The resulting images are rendered in pseudo-color to show the correlation between specific activities and brain function [8]. Several studies have shown that PET/CT images are more effective than PET or CT alone and can aid in better detecting pathologies, especially for less experienced health professionals [9].

1.3. Color segmentation methods

Color segmentation approaches can be extended from grayscale methods and are covered comprehensively in several surveys found in literature [10,11,12]. These results show that utilizing all color channels of a pixel can produce better results than grayscale methods that utilize only a single channel per pixel [13,14]. However, as shown by the literature, the use of colorization to improve segmentation is still a highly researched topic and one that shows potential. Color segmentation is performed on generic digital images as well as digital medical images. A popular approach is color region growing that uses the spatial and color intensity information found in the image to segment the region. Color region growing examines neighbor pixels of the region of interest (ROI), if the neighboring pixel fulfills a spatial and color intensity criterion the pixel is added to the ROI. Basic color region growing methods are fast and easy to implement. These methods utilize the spatial and color information found in the image and does not require training. One of the drawbacks of color region growing methods is their susceptibility to noise: they are not as effective when the values of ROI and the values of the background image are similar. To compensate for their drawbacks color region growing methods can be implemented with advanced segmentation approaches.

Tremau and Borel [15] developed a color region growing and merging algorithm in RGB space. In the method the image is partitioned into regions based on spatial and color information. These regions are merged if they are colorimetrically homogeneous. Shih and Cheng [16] developed a color region growing algorithm where they converted the RGB image into a color space defined by luminance (Y), and the red and blue reference values (YC_bC_r). Seeds were placed in the image automatically based on the neighboring pixels and the number of connected/disconnected regions. The seeds labeled their pixel neighbors into corresponding regions. The process was repeated for every pixel until all pixels were classified. If the color similarity of two regions was under a predefined threshold the regions were combined. These methods were tested on generic digital images and not digital medical images.

Segmentation of color images has also been successfully applied to medical images. Gomez et al. [17] developed an advanced automatic color seeded region growing method using instance-based learning. For each color band in the image a histogram was generated, divided, and grouped into subintervals. A pixel was considered a seed if the gray values of the pixel in each band fell in a representative interval. The instance-based algorithm used the seeds for region growing. This method was applied in medical images to detect leukemia. Fondon et al. [18] developed an advanced color multistep region growing method that utilized the color intensity information and the texture information of the color image. A region of interest was selected and used as the reference to extract color and texture information. Seeds were placed automatically if they had the desired color and texture. For every seed, region growing began by

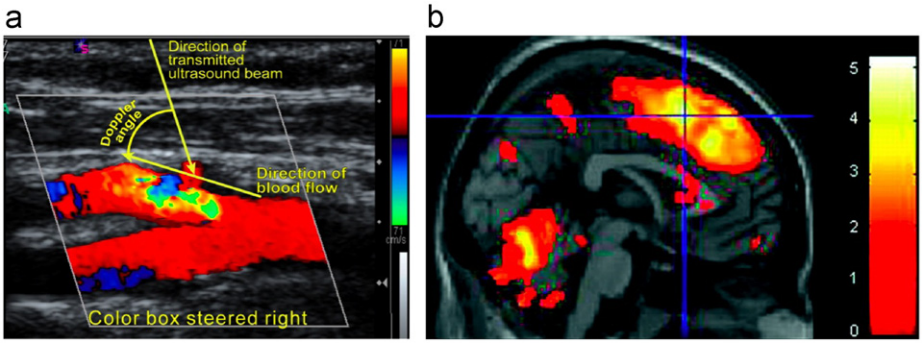

Fig. 1. Examples of colorized digital medical image data. (a) Color Doppler of a blood flow in the carotid arteries [10]; (b) Brain fMRI to study the effects of pain stimuli in irritable bowel syndrome [11]. (For interpretation of the references to color in this figure caption, the reader is referred to the web version of this article.)

examining neighbor pixels. A pixel was selected as part of the region if: (1) the pixel was not part of another region, (2) the texture of the pixel was under a threshold, and (3) the new pixel was similar in color intensity to the pixels already in the region. If the final region was not optimal the region growing process was repeated with new thresholding values.

Because of the challenges of current color medical imaging technologies most tumor segmentation techniques are based on grayscale methods. Using colorization methods, it is possible to transform a digital medical image into a color space to then apply color segmentation. Tavakol [19] colorized infrared thermal images of the breasts to improve the detection of tumors. The images were colorized by a pseudo-color coding method based on the CIELAB color space and then segmented using a fuzzy *c*-means method and *K*-means method. Juang and Wu [20] applied a color *K*-means segmentation algorithm on a color converted image and obtained successful results for gliomas.

Although these methods did not conclusively demonstrate that colorization of grayscale medical image data significantly improves segmentation, the results are encouraging and shows promise for future applications. These methods were applied on image data that is fairly consistent in texture and shape (e.g., infrared breast images, brain MRI). Further investigation on more complex images such as abdominal scans would help in determining the benefits of colorizing grayscale medical image data prior to performing segmentation.

1.4. Motivation

Color segmentation approaches utilize the multichannel information found in every color pixel without drawbacks of processing times. Color segmentation methods can potentially produce better segmentation results than grayscale methods for medical images. However, as discussed, most research in image colorization is not being done on digital medical images. Before advanced techniques can be developed and implemented, it first needs to be determined if colorizing digital medical before segmentation is beneficial. Colorization, as defined here, is the process of converting an image from the grayscale space into a color space. The work presented in this paper investigates whether colorization can significantly increase segmentation accuracy in CT images while remaining easy to use, fast, and require only commodity computational resources.

2. Methodology

The developed method is semi-automatic and is composed of three steps: (1) colorization, (2) segmentation, and (3) post-processing.

2.1. Colorization

The method is initialized with the user selecting a Region of Interest (ROI) around the tumor on the first slice of the CT data set. This ROI selection identifies the tumor from the healthy tissues, where the maximum and minimum tissue density Houndsfield Units (HU) of the ROI were obtained and set as the range of pixels to be colorized. The ROI does not have to accurately match the tumor size and shape, but for a complex dataset, such as a highly calcified tumor with heterogeneous tissue densities, the ROI has to completely include the tumor in the first slice for the colorization process to be effective. For homogenous tumors, it was found that the ROI did not have to fully contain the tumor, since a small piece of the tumor was sufficient to represent the complete tissue range of the tumor and to differentiate the tumor from healthy tissues. Once the ROI is selected, tissue densities that were not included in the ROI range were set to black and assumed to be non-tumor tissues. These pixels were ignored in the segmentation process decreasing computational time and allowing the method to run on a standard desktop or laptop computer.

Each grayscale pixel was assigned a color value (R, G, B) based on a generated color map. To generate the color map, the variable V is calculated as the ratio of the pixel's tissue density (HU value) and the tissue density range of the ROI. Expanding on a method introduced by Gonzalez et al. [24], a color scheme was developed where the lowest tissue density value was colored red, blending towards green as the tissue density value increases and continue to blend from green to blue for the next range of increasing tissue densities. This process converts the tissue densities into 8-bit color pixels of red, green, and blue channels.

Thus, if V was less than 0.5, the blue value of the pixel to be colorized, $V_{\text{blue,}}$ was set to 0, and the red and green values, V_{red} and V_{green} respectively, were assigned as shown in the following equation:

$$V_{\text{red}} = 255(1-2V)$$
$$V_{\text{green}} = 255(2V) \quad (1)$$

If V was more than or equal to 0.5, the red value of the pixel to be colorized was set to 0, and the green and blue values were set as shown in the following equation:

$$V_{\text{green}} = 255[(1-2(V-0.5)]$$
$$V_{\text{blue}} = 255[(2(V-0.5)] \quad (2)$$

This color mapping was developed so that tissues close in range with the tumor had similar RGB values. Pixels that had a value close to the minimum HU value of the tumor were set mainly to red, and pixels that were close to the maximum HU value were set mainly to blue. Mapping it in this manner allowed for enhanced contrast of the tumor and healthy tissues. In addition, the mathematics was purposefully kept simple to reduce computational load. More complex mappings can be done, but could significantly increase computational time, thus requiring more than commodity hardware. This simple formulation combined with textures in OpenGL allows the colorization to be adjusted in real time to improve the contrast between the tumor and the healthy tissues. The textures of OpenGL are analogous to creating and slapping a sticker of the data to the screen, it is faster than drawing an image pixel by pixel and allows a user to see results in real time. The goal of this step is not to realistically color the anatomy but rather to use color to accentuate the gradients between tumors and healthy tissue to improve segmentation. An example of the colorization process after adjustments is shown in Fig. 2. The figure on the left shows the original CT image in grayscale and the figure on the right shows the final results of the colorization process. The actual tumor (from gold standard) is highlighted in the dotted yellow line as a reference.

2.2. Color thresholding segmentation

To investigate the effectiveness of colorization in tumor segmentation, a basic thresholding segmentation algorithm was applied. It is important to state that thresholding segmentation is not widely used and is seen as an older, less effective method than others segmentation methods. However, this proves a good test method as it was theorized that the addition of color information could vastly improve segmentation results, even with a primitive method such as thresholding.

A threshold factor, F, was computed from the colorized space by (1) a color component, which is the difference in the red, green and blue channel color values of the pixel to the average RGB

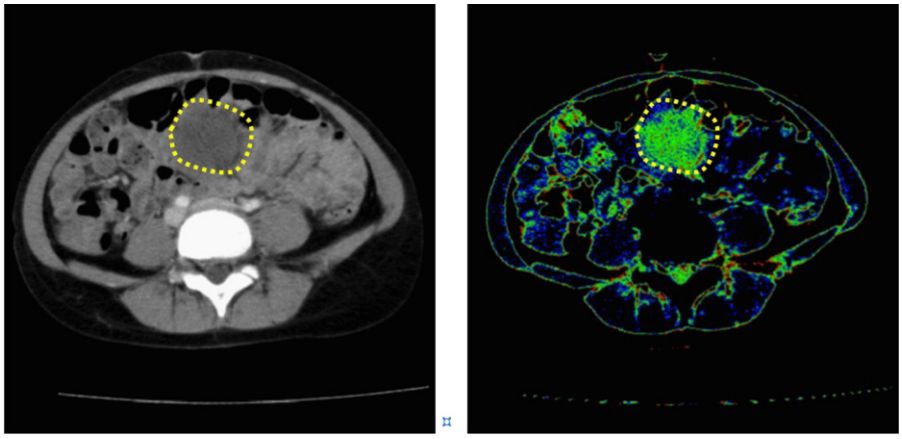

Fig. 2. Colorization process: (Left) Original CT image visualized in grayscale. (Right) Final image after colorizing and adjustments, tissues that fall outside of the tissue range of the tumor are set to black. Tumor is outlined in yellow. (For interpretation of the references to color in this figure caption, the reader is referred to the web version of this article.)

values of the entire ROI and (2) a spatial component from each pixel to the center of the ROI (i.e. the seed point).

The color component is the difference between the ROI's average values in the red, green, and blue channels and the current pixel's red, green, and blue values respectively as shown in the following equation [19]:

$$I_p = \|V_{rgb} - I_{rgb_{ROI}}\| = \frac{\left[(V_{\text{red}} - I_{\text{red\_ROI}})^2 + (V_{\text{green}} - I_{\text{green\_ROI}})^2 + (V_{\text{blue}} - I_{\text{blue\_ROI}})^2\right]^{1/2}}{255} \tag{3}$$

$I_{\text{red\_ROI}}$, $I_{\text{green\_ROI}}$, $I_{\text{blue\_ROI}}$ are the average values of the intensities in the red, green, and blue channels respectively inside the ROI.

V_{red}, V_{green}, V_{blue} are the pixel's red, green, and blue channel intensity values respectively.

The spatial component is the ratio between the distance of the pixel from the seed, r_{pixel}, and the search region, $r_{\max}$, as shown in the following equation:

$$D = \frac{r_{\text{pixel}}}{r_{\max}} \tag{4}$$

For the first slice the seed was placed at the center of the ROI and the distance of the pixel from the seed, r_{pixel}, was computed by

$$r_{\text{pixel}} = \sqrt{(x_{\text{seed}} - x_{\text{pixel}})^2 + \left(y_{\text{seed}} - y_{\text{pixel}}\right)^2} \tag{5}$$

To take into account the tumor variation in size and location throughout the slices, the seed is automatically moved in each slice and placed at the center of the previous slice's segmented region. It was assumed that the tumor did not vary significantly between consecutive slices and placing the seed at the center of the previous slice's segmented region was enough to account for the variability of the tumor from each slice. If the need arises to account for larger variations in tumor shape and location, there is significant research in image registration that could be added to aid in this issue.

In addition to seed placement, the search region, $r_{\max}$, had to take into consideration the change in size and location of the tumor. The search region was then updated in each slice using:

$$r_{\max} = SC_i \tag{6}$$

where S is the search region, of the previous slice. C_i is the percentage of the tumor's change in size and is defined as

$$C_i = \frac{3E_{i-1} + 2E_{i-2} + E_{i-3}}{6} \tag{7}$$

where $i-1$ represents the previous slice, $i-2$ represents the second previous slice, and $i-3$ represents the third previous slice. E is the growth rate of the tumor in the previous slice and is defined as

$$E_i = \frac{\text{Radius of segmented region of slice } i}{\text{Radius of segmented region of slice } i-1} \tag{8}$$

To calculate C_i, region information from previous slices is needed. This calculation can be completed from the fifth slice onwards. For slices one through four, a user-defined growth rate was used. For this research a default value of 10% was used.

Using the color component and the spatial component the thresholding factor was calculated as

$$F = I_p \times D \tag{9}$$

A pixel was selected as tumor if its thresholding factor was lower or equal to the original threshold value of 10%.

Results of an initial segmentation are shown in Fig. 3. Fig. 3a shows the original grayscale image. Fig. 3b shows the image after colorization as well as the location of the seed point to be used for segmentation. Fig. 3c shows the final segmentation results before additional adjustments. The yellow dotted lines shown in Fig. 3a and c are not the ROI selected but were added to illustrate the actual tumor within the image as a reference.

2.3. Post-processing

This post-processing involved implementing erosion and dilation morphological operations on the segmented regions to eliminate segmentation noise, using a 5×5 square structuring element. The erosion process removed stray disconnected regions that are smaller than 5×5 pixels, while the dilation process filled in "holes" within the segmented regions that are smaller than 5×5 pixels [21,23].

2.4. Real time adjustments

The tissue density range from the region of interest selected during initialization can be adjusted to improve the segmentation results. This step allows the tissue density range from the region of interest used for colorization to be adjusted to improve the segmentation results. Fig. 4 shows an example of such a case, the yellow dashed lines outline the tumor (as defined by the gold standard) and red is the segmentation result. In this case the method failed to recognize most of the pixels in the tumor, producing a high false negative error. By adjusting the range of tissue densities to be

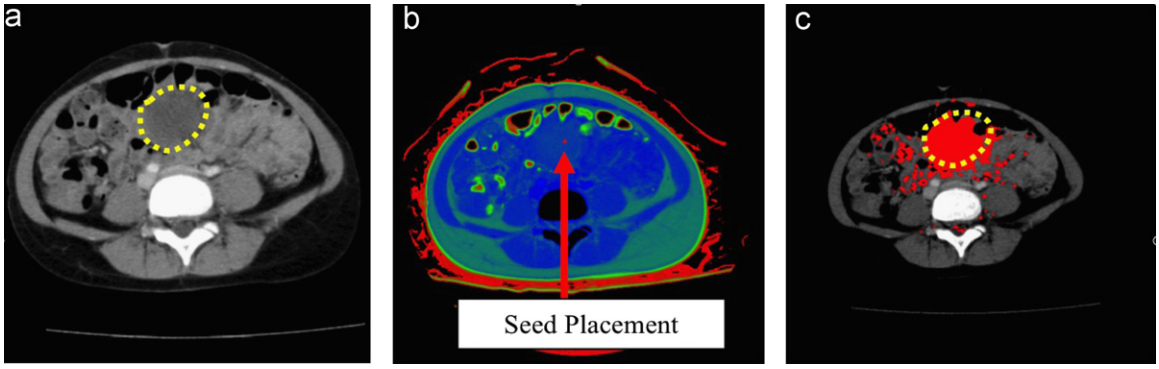

Fig. 3. Segmentation process: (a) original grayscale image, (b) seed placement on the colorized image, and (c) initial tumor segmentation. (For interpretation of the references to color in this figure caption, the reader is referred to the web version of this article.)

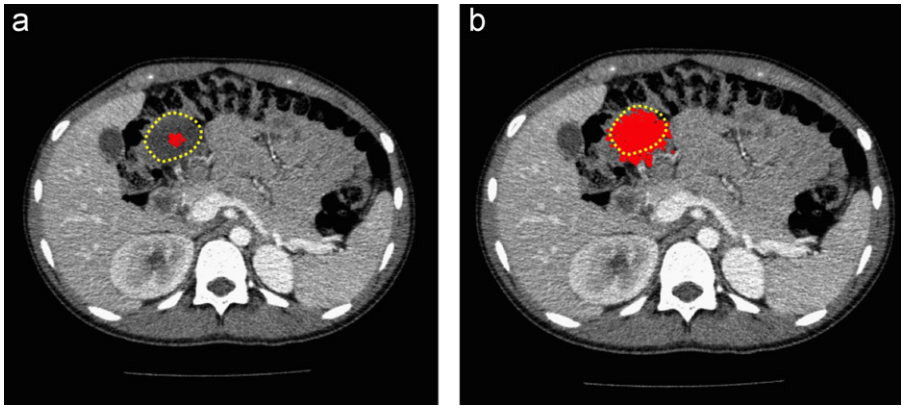

Fig. 4. The results of the segmentation (a) can be refined in real time to obtain better segmentation results (b). (a) Initial segmentation and (b) Segmentation after refinement. (For interpretation of the references to color in this figure caption, the reader is referred to the web version of this article.)

colorized, different pixels could be added to the segmented object of the current slice. Because pixels that were not part of the range were ignored, adjusting the parameters was extremely fast allowing the results to be displayed in under a second for the current slice. This was accomplished by a simple user interface that allowed the user to change the minimum and maximum values of the tissue density range from the region of interest and see the colorization applied in real time for a single image slice. A series of 100 slices required an average of 1.9 s to recolor and regenerate the segmentation results. This adjustment process is user dependent, placing the decision making process in the hands of the user and assumes that they have knowledge of the tumor being segmented.

2.5. Grayscale segmentation

To generate the grayscale image, the data is scaled into an 8-bit intensity map using the following equation for V:

$$V = \frac{\text{tissue density}}{\text{maxtissue density} - \text{mintissue density}} \times 255 \tag{11}$$

The procedure for grayscale segmentation is almost identical to the color segmentation procedure except for Eq. (3), which is now replaced by the following equation:

$$I_p = \|V - I_{\text{ROI}}\| \tag{12}$$

where I_{ROI} is the average grayscale intensity of the ROI.

2.6. Description of test datasets and procedure

Ten different datasets from seven individuals were used to test the method. Dataset #1 is a Cystic Teratoma on the left ovary, #2 is an immature Teratoma, #3 is a Mucinous Cystadenoma on the right ovary, and datasets #4–#10 are Neuroblastomas. A summary of the datasets is provided in Table 1.

For the purpose of this research, the datasets were categorized into three groups based on their characteristics. Tumors that had homogeneous densities were classified as category A; tumors that had fuzzy edges and had some inhomogeneity in their tissues were category B; and tumors that had heterogeneous tissues were designated category C. Tumors with calcium buildup are designated category B or C depending on the degree of calcification. Manual segmentations were obtained from radiologists as the gold standard to evaluate the performance of the method.

The segmentation method was performed using Matlab on a system with Dual AMD Opteron 250 2.4 GHz processors, 4 GB of memory, dual 512 MB NVidia Quadro FX4500 graphics cards, and running Linux Red Hat Enterprise 5.1.

The accuracy was measured by calculating the misclassification rates of the pixels. If the segmentation algorithm classified a pixel as part of the tumor but it was not part of the golden standard that pixel was considered a False Positive (FP). If a pixel that was part of the tumor according to the gold standard but was not selected by the algorithm then that pixel was considered a False Negative (FN). Both rates were calculated with the equations below multiplied by 100%:

$$FP = \frac{V(A) - V(A \cap R)}{V(R)} \tag{11}$$

$$FP = \frac{V(R) - V(A \cap R)}{V(R)} \tag{12}$$

where $V(R)$ was the volume segmented by the radiologist, the golden standard, $V(A)$ was the volume segmented by the method,

Table 1
Summary of the tumor CT datasets.

#	Description	# Segmented slices	Category
1	Cystic Teratoma on left ovary	19	A
2	Mucinous Cystadenoma on right ovary	251	A
3	Immature Teratoma	90	A
4	Neuroblastoma, small and diffuse	4	B
5	Neuroblastoma	31	B
6	Neuroblastoma	12	C
7	Neuroblastoma, some calcification	13	B
8	Neuroblastoma, some calcification	23	C
9	Neuroblastoma, highly calcified	16	C
10	Neuroblastoma	17	C

Table 2
Averages of the results of the 10 datasets in both color and grayscale methods and results of the t-test ($p < 0.05$).

	Color	Grayscale		Color	Grayscale	
Dataset	**FP (%)**	**FP (%)**	***p*-value**	**FN (%)**	**FN (%)**	***p*-value**
1	21	51	< 0.001	5	1.77	0.140
2	8	32	0.014	10	3.24	< 0.001
3	13	41	< 0.001	29	62	0.013
4	134	665	< 0.001	40	33	0.421
5	57	116	0.002	27	61	0.005
6	53	738	< 0.001	35	38	0.669
7	31	108	0.173	41	72	0.004
8	37	135	< 0.001	54	29	< 0.001
9	28	198	< 0.001	59	74	0.035
10	31	246	< 0.001	43	10	< 0.001

and $V(A \cap R)$ is the intersection of the segmented region and the gold standard. In addition, the seven users also performed two runs using thresholding without colorization. This provides data to compare how the colorization improved segmentation. A statistical t-test ($p < 0.05$) was also performed to test the hypothesis of whether the colorization process improved the segmentation results.

3. Results and discussion

The 10 datasets were segmented both with and without colorization. Every part of the segmentation process was the same, except no color information was present for the grayscale segmentation runs. For grayscale, the initial region selected by the user determined the average HU value. This average was then compared to the value of each pixel and was used as the "color" component of Eq. (5). This component was combined with the search region to produce the threshold factor. The average results combined with the color results are shown in Table 2, which demonstrates improvements in segmentation accuracy when the proposed colorization process was employed prior to segmentation.

A t-test ($p < 0.05$) was performed on the results (both colorization and grayscale) for all 10 datasets to evaluate their statistical significance. The t-test results indicated strong evidence that the colorization method had better results than the grayscale method. For the FP, the color method performed significantly better in nine of the 10 datasets, as shown by the *p*-values. For the FN values the colorization method gave significantly better values for four out of the 10 datasets.

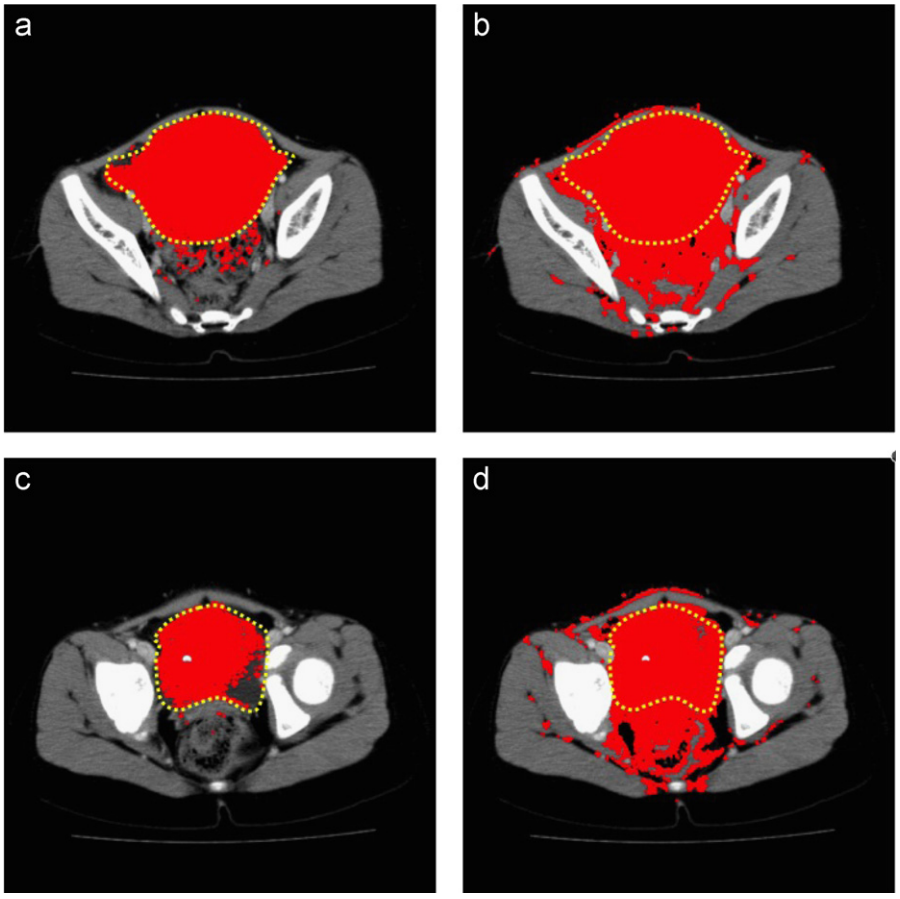

Fig. 5. Dataset #1 Yellow outlines the approximate tumor, red is the actual segmentation by the algorithm. Grayscale case selects many pixels that are not part of the tumor resulting in high FP values. (a) Dataset #1 colorization, slice #44, (b) Dataset #1 grayscale, slice #44, (c) Dataset #1 colorization, slice #49 and (d) Dataset #1 grayscale, slice #49. (For interpretation of the references to color in this figure caption, the reader is referred to the web version of this article.)

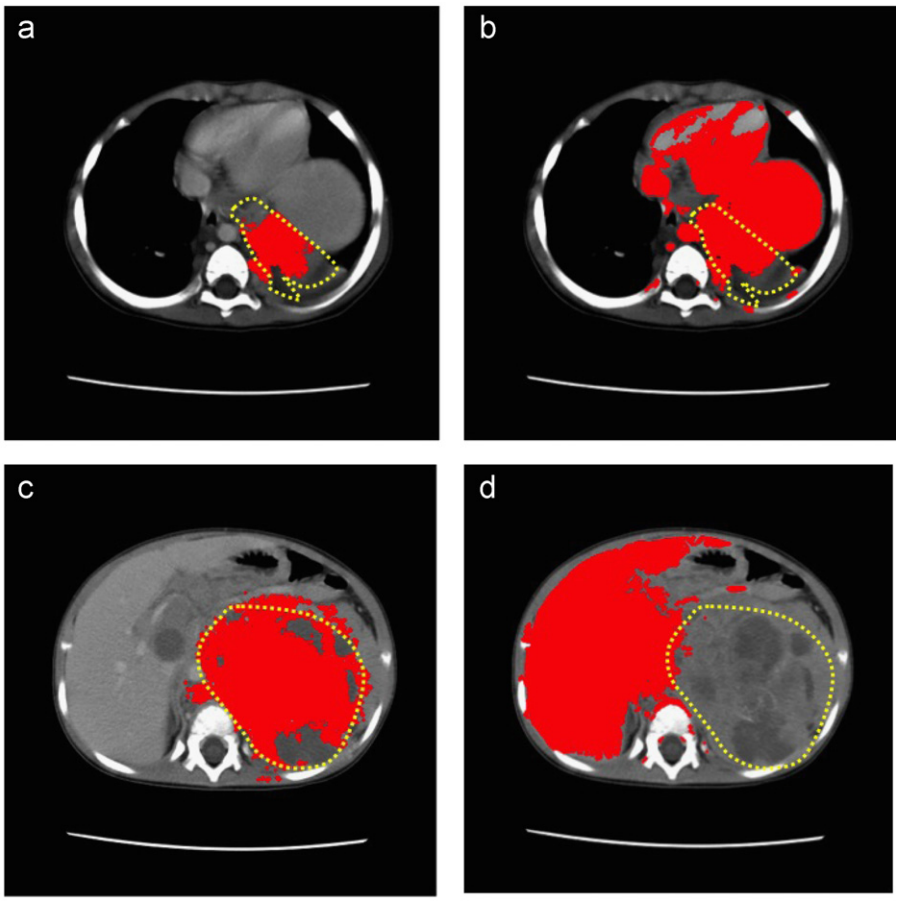

Fig. 6. Dataset #5 Yellow outlines the tumor, red is the segmentation by the algorithm. Grayscale method selected many pixels that are not part of the tumor resulting in high FP values. The grayscale method leaks and the tumor pixels are not segmented (shown in b and d). (a) Dataset #5 colorization, slice #18, (b) Dataset #5 grayscale, slice #18, (c) Dataset #5 colorization, slice #38 and (d) Dataset #5 grayscale, slice #38. (For interpretation of the references to color in this figure caption, the reader is referred to the web version of this article.)

For two datasets in which the colorization method performed worse with higher FN values, the t-test did not show any statistical significant differences. Only three of the datasets produced better FN results for the grayscale method that were statistically significant different but these same datasets also gave much higher FP values for the same datasets. On closer examination, the grayscale algorithm selected many of the pixels in the image even if they were not part of the tumor, resulting in low FN values but increasing their FP values significantly. An example is shown in Fig. 5, where the grayscale method over-segmented the image, increasing the number of pixels that were part of the tumor, which produced a lower FN value, but increasing the number of pixels that were not part of the tumor, producing a high FP value. The takeaway is that even though statistically FN values were better for the grayscale method, it produces a substantially higher percentage of FP error compared to colorization.

The grayscale method was not capable of segmenting the right pixels for category B tumors that had fuzzy edges and heterogeneous tissues at all, as shown in Fig. 6. However, the colorization process has improved the segmentation results, segmenting most of the actual tumor. Comparing results for both methods, the grayscale thresholding suffered from a high false positive error selecting mostly healthy tissues. This could be due to the healthy tissues having very similar tissue densities as the tumor tissues, thus translating to similar grayscale intensities.

Category C tumors that were calcified and heterogeneous had tumor pixels of different values than the healthy tissues, but the grayscale method was not able to take advantage of the different values and was not able to segment the tumor tissues. Even when there is a different gradient between two tissues, grayscale pixel values were not sufficient to produce good segmentation results. These results are shown in Fig. 7. Again, colorization was able to improve the results as seen in the figure.

Histogram analyses were done on all the datasets and showed that the datasets were of varying multi-modal distributions. In addition, histogram analyses were also performed on the ROIs of the datasets and the results were a mix of uni-modal and multi-modal distributions, specifically for tumors that are highly calcified.

The results presented demonstrate a dramatic improvement in segmentation results after the colorization process, especially after real time adjustment of the tissue density range from the region of interest. The re-colorization process after this process is performed in real time, and the recalculation of the segmentation results is on average 1.9 s per 100 image slices. The colorization process accentuates the tissue contrast within the image and also limits the range of tissue density that will be examined for segmentation. If colorization prior to segmentation improves basic segmentation methods with statistical significant difference, then it is hypothesized that advanced intensity based segmentation methods could benefit from colorization enormously as well. The potential to improve segmentation accuracy while maintaining efficient and close to real time performance will lead to faster case diagnosis and improve patient care.

4. Conclusions

A framework to colorize CT images for tumor segmentation was presented. As proof of concept a basic color region growing

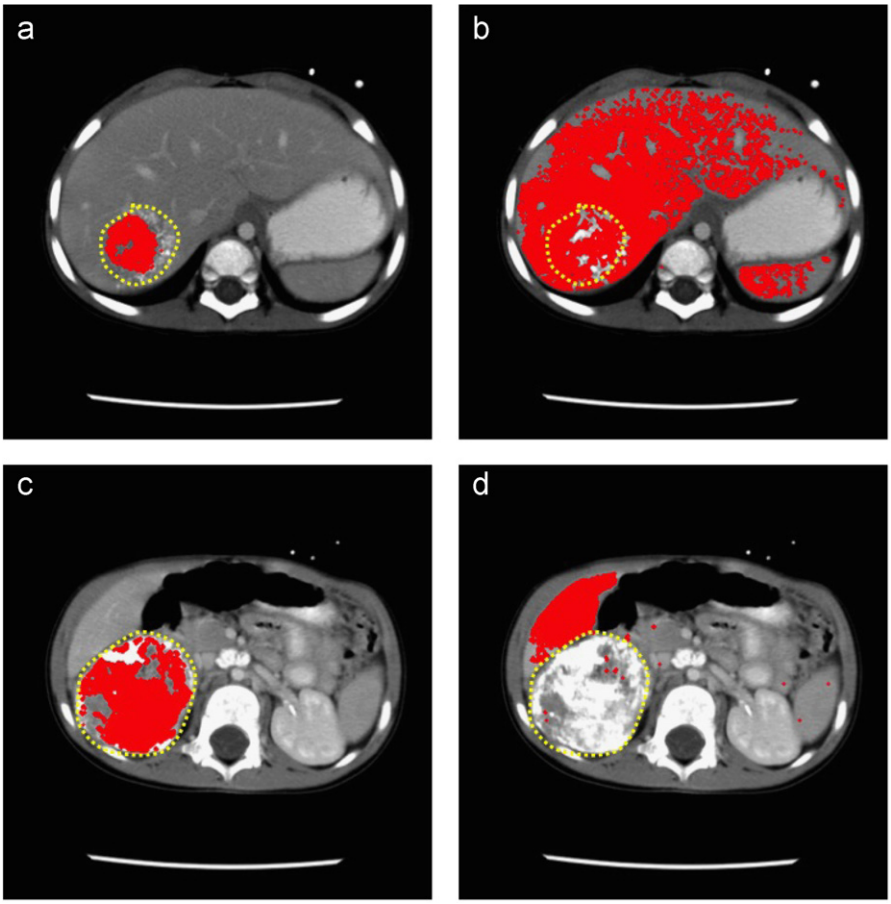

Fig. 7. Dataset #9 Yellow outlines the approximate tumor, red is the actual segmentation by the algorithm. Grayscale method selects many pixels that are not part of the tumor resulting in high FP values. For the last slices the grayscale method leaks and most of the tumor is not selected (shown in b and d). (a) Dataset #9 colorization, slice #28, (b) Dataset #9 grayscale, slice #28, (c) Dataset #9 colorization, slice #39 and (d) Dataset #9 grayscale, slice #39. (For interpretation of the references to color in this figure caption, the reader is referred to the web version of this article.)

technique was implemented with and without a colorization method. The original data was first colorized into a RGB space and a region growing method was implemented using this colorized data. The method was compared to the same region growing approach but using the original grayscale data. The colorization method performed significantly better in most test cases. Statistical *p*-values were calculated for every dataset and produced strong evidence that the differences were statistically significant. In addition the color region growing segmentation method took under 1 s per slice on commodity hardware to process. These results offer proof that using color in medical images can significantly improve tumor segmentation accuracy.

5. Future work

Future work will involve adding more advanced segmentation algorithms to the colorization method, such as a probabilistic method algorithm or fuzzy segmentation. In addition, additional pre-processing steps such as intensity inhomogeneity correction (IIC) could further improve colorization mapping and the resultant segmentation. Lastly, investigation of different color maps on the segmentation algorithms, converting from the RGB space to HIS and segmenting the image in the HIS space has been developed before and could be a viable option [22]. The method in which the ROI is moved between consecutive slices will also have to be improved to account for abrupt changes in shape, size, or location of the tumor.

Conflict of interest statement

None declared.

Acknowledgments

The authors would like to thank Dr. G. Miyano from Juntendo University School of Medicine, Tokyo, Japan and Dr. R.M. Rangayan from University of Calgary, Alberta, Canada for providing the datasets used as test cases, and radiologists Dr. J.L. Friese from Brigham and Women's Hospital, Boston, Massachusetts and radiologist Dr. G.S. Boag from Alberta Children's Hospital, Calgary, Canada for providing the manual segmentations that were used as the gold standard.

References

[1] A. Levin, D. Lischinski, Y. Weiss, Colorization using optimization, in: Proceedings of the 2004 SIGGRAPH Conference, 2004, vol. 23(3), pp. 689–694.
[2] T. Welsh, M. Ashikhmin, K. Mueller, Transferring color to greyscale images, in: Proceedings of the 29th Annual Conference on Computer Graphics and Interactive Techniques, 2002, vol. 21(3), pp. 277–280.
[3] T. Horiuchi, S. Hirano, Colorization algorithm for grayscale image by propagating seed pixels, in: International Conference on Image Processing, 2003, pp. 457–460.
[4] Y. Qu, T. Wong, P. Heng, Manga colorization, in: Proceedings of the 2006 SIGGRAPH Conference, 2006, vol. 25(3), pp. 1214–1220.
[5] X. Liu, J. Liu, Z. Feng, Colorization using segmentation with random walk, in: Computer Analysis of Images and Patterns, 2009, vol. 5702(2009), pp. 468–475.

[6] K. Parker, M. Zhang, D. Rubens, An introduction to color in medical imaging., J. Imag. Sci. Technol. 50 (1) (2006) 12–15.
[7] R. Omoto, et al., The development of real-time two-dimensional Doppler echocardiography and its clinical significance in acquired Valvular diseases., Jpn. Heart J. 25 (3) (1984) 325–340.
[8] K. Kwong, et al., Dynamic magnetic resonance imaging of human brain activity during primary sensory stimulation, Proc. Natl. Acad. Sci. 89 (12) (1992) 5675–5679.
[9] J. Czernin, M. Allen-Auerbach, H.R. Schelbert, Improvements in cancer staging with PET/CT: literature-based evidence as of September 2006, J. Nucl. Med. 48 (1) (2007) 78S–88S.
[10] H.R. Tahmasebpour, A.R. Buckley, P.L. Cooperberg, C.H. Fix, Sonographic examination of corotid arteries, Radiographics 25 (6) (2005) 1561–1575.
[11] S. Elsenbruch, et al., Affective disturbances modulate the neural processing of visceral pain stimuli in irritable bowel syndrome: an fMRI study, Gut 59 (4) (2008) 489–495.
[12] D.L. Pham, C. Xu, J.L. Prince, Current methods in medical image segmentation, Annu. Rev. Biomed. Eng. 2 (2000) (2000) 315–337.
[13] W. Skarbek, A. Koschan, Colour Image Segmentation: A Survey Technical Report, Technical University of Berlin, October 1994.
[14] H. Palus, Color image segmentation: selected techniques, in: Color Image Processing: Methods and Applications, CRC Press, Boca Raton, 2006, pp. 103–128.
[15] L. Lucchese, S.K. Mitra, Colour image segmentation: a state-of-the-art survey, in: Proceedings of the Indian National Science Academy, 2001, vol. 67(2), pp. 207–221.
[16] H.D. Cheng, X.H. Jiang, Y. Sun, J. Wang, Color image segmentation: advances and prospects, Pattern Recognition 34 (12) (2001) 2259–2281.
[17] A. Tremeau, N. Borel, A region growing and merging algorithm to color segmentation, Pattern Recognition 30 (7) (1997) 1191–1203.
[18] F. Shih, S. Cheng, Automatic seeded region growing for color image segmentation, Image Vision Comput. 23 (10) (2005) 877–886.
[19] O. Gomez, J. Gonzalez, E. Morales, Image segmentation using automatic seeded region growing and instance-based learning, Prog. Pattern Recognition Image Anal. Appl. 4756 (2007) 192–201.
[20] I. Fondon, C. Serrano, B. Acha, Color-texture image segmentation based on multistep region growing, Opt. Eng. 45 (5) (2006) 057002.
[21] E. Tavakol, S. Sadri, E.Y.K. Ng., Application of K- and fuzzy c-means for color segmentation of thermal infrared breast images, J. Med. Syst. 34 (1) (2010) 35–42.
[22] L. Juang, M. Wu, MRI brain lesion image detection based on color-converted *K*-means clustering segmentation, Measurement 43 (2010) (2010) 941–949.
[23] R.M. Haralick, L.G. Shapiro, Computer and Robot Vision, vol. I, Addison-Wesley, New York, 1992, pp. 174–188.
[24] R.C. Gonzalez, R.E. Woods, Digital Image Processing, Addison-Wesley, New York, 2008.